



Porous zirconium phosphate supported tungsten oxide solid acid catalysts for the vapour phase dehydration of glycerol



Ginjupalli Srinivasa Rao, N. Pethan Rajan, M. Hari Sekhar,
S. Ammaji, Komandur V.R. Chary*

Catalysis Division, Indian Institute of Chemical Technology, Hyderabad, India

ARTICLE INFO

Article history:

Received 10 April 2014

Received in revised form

11 September 2014

Accepted 14 September 2014

Keywords:

Porous zirconium phosphate (ZrP)

Tungsten oxide

Glycerol

Acrolein

Dehydration

ABSTRACT

Solid acid catalysts containing WO_x/ZrP with varying the active component loading (5–40 wt%) on porous ZrP support have been investigated for the vapour phase dehydration of glycerol to acrolein. The catalyst containing 30 wt% WO_x/ZrP has shown high selectivity to acrolein (about 82%) with a total conversion of glycerol at 300 °C in the presence of water. The calcined catalysts were characterized by X-ray diffraction, pore size distribution, FT-IR, UV-DRS, pyridine adsorbed FT-IR and NH_3 -temperature programmed desorption to elucidate the structural and acidic properties of the catalysts. The XRD results suggest that WO_x is found to be present in a highly dispersed state at lower loadings (<30 wt%) and crystalline WO_x at higher loadings. NH_3 -TPD and FT-IR results of adsorbed pyridine suggest that the total acidity and number of Brønsted acidic sites are found to increase with WO_3 loading on the support. Further, there is no significant change of acidity was noticed at higher loadings. The conversion of glycerol and the selectivity toward acrolein mainly depend on the fraction of moderate acidic sites and Brønsted acidic sites. The Glycerol dehydration functionalities are explained in terms of the acidity and structural properties of WO_x/ZrP catalysts. In addition, the positive effect due to addition of air to N_2 feed flow suppresses the coke formation on the surface of catalyst was also investigated during dehydration reaction.

© 2014 Elsevier B.V. All rights reserved.

1. Introduction

Renewable biomass resources are promising alternatives for the sustainable synthesis of chemical intermediates and liquid fuels [1]. The by-product produced in bio-diesel synthesis is glycerol and its effective utilization will be a key issue to promote the bio-diesel commercialization. Therefore, new uses of glycerol need to be explored for its valorization. The crude glycerol can be converted to acrolein, which is an important chemical intermediate for the production of acrylic acid, acrylic acid esters, super absorbers and polymers [2,3]. Acrolein is also used for the manufacture of methionine, 1,3-propanediol, glutaraldehyde, pyridines, flavors, and fragrances [4]. Compared to the petroleum-based processes [5], the dehydration of glycerol to acrolein has received a great deal of attention in the recent past as a significant route by virtue of its being an environmentally benign process.

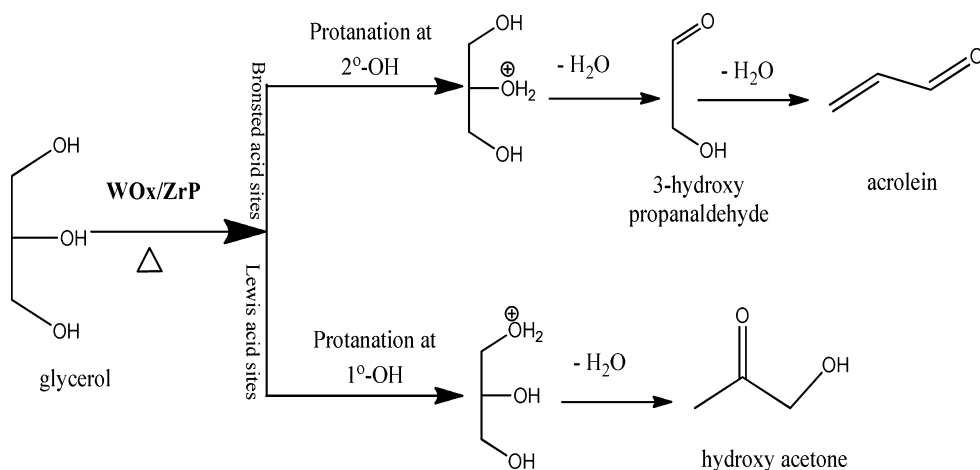
The dehydration of glycerol in gas phase on acidic catalysts is a typical example of double dehydration reaction proceeds via the

formation of 3-hydroxypropionaldehyde and 1-hydroxyacetone [6] (**Scheme 1**). The highest selectivity to acrolein reported so far in both the vapour phase and liquid phase dehydration process is 65–90%. It was found that a solid acid with Hammett acidity (H_o) between –10 and –16 is the most suitable catalyst for the dehydration of glycerol than the catalysts having lower acidity with H_o between –2 and –6 [7]. However, such strong acidic catalysts are known to deactivate rapidly due to deposition of carbonaceous species on the catalyst surface [8]. The acidic properties in combination with textural properties of the catalysts in the presence of large number of micro pores also play an important role in determining the catalytic performance [9–13]. The selectivity and deactivation during glycerol dehydration will be strongly affected by diffusion constraints due to coke formation.

The dehydration of glycerol to acrolein in the gaseous phase over a solid acid catalyst leads to a sufficiently high dehydration activity. However the catalyst deactivation is a major concern due to severe reaction conditions, coke formation [8,14–16], sintering or leaching of active phase in the reaction media [17] and formation of large amount of by-products.

Among various solid acid catalysts reported, WO_3/ZrO_2 catalysts represent one of the highly active catalysts for vapour

* Corresponding author. Tel.: +91 40 27193162; fax: +91 40 27160921.
E-mail addresses: kvrchary@ict.res.in, Charykvr@gmail.com (K.V.R. Chary).



Scheme 1. Schematic representation of the dehydration of glycerol to acrolein and acetol.

phase dehydration of glycerol, as they exhibit show unique catalytic performance in the dehydration of glycerol [18–20]. Ulgen and Hoelderich [18] have evaluated the catalytic performance of WO_3/ZrO_2 catalysts with various WO_3 loadings and noticed an increase of acrolein selectivity in 73% with 19 wt% catalyst. Similar acrolein selectivity was also reported at 300 °C with total conversion using a commercial WO_3/ZrO_2 catalyst [19]. On the other hand improvement of tungstated zirconia catalyst with SiO_2 doping, exhibited better acrolein selectivity (80%) with long catalyst life and thermal stability to the catalyst [20]. There are many investigations reported on the structural and acidic properties of WO_x/ZrO_2 solid acids for glycerol dehydration reaction. However, not many studies reported so far on the interaction of WO_x with porous zirconium phosphate support for the gas phase glycerol dehydration reaction.

In the present study we report the synthesis, characterization and application of porous zirconium phosphate (ZrP) supported WO_x catalysts for the dehydration of glycerol to acrolein. Our results provide mainly a basis for correlating the catalyst acidity by varying the tungsten oxide content and the effect of reaction temperature in glycerol dehydration. In addition, we also report the positive effect due to addition of air to reactant flow in the gas phase dehydration of glycerol.

2. Experimental

Porous zirconium phosphate support was prepared from zirconium n-propoxide precursor and 85% phosphoric acid following the procedure described elsewhere [21]. About 0.01 mol of zirconium n-propoxide, (70 wt% solution in 1-propanol, Aldrich) was added drop wise to a 60 mL solution of H_3PO_4 (0.1 mol L⁻¹) under stirring. After 2 h of stirring at room temperature, the obtained mixture was transferred into a teflon lined autoclave and aged statically at 80 °C for 24 h. The final material was filtered, dried and calcined at 400 °C for 5 h. A series of WO_x/ZrP catalysts with WO_x loadings ranging from 5 to 40 wt% supported on ZrP were prepared by impregnation method by adding aqueous solution of ammonium metatungstate to the calcined ZrP support. The catalysts were subsequently dried at 100 °C for 12 h and calcined in a muffle furnace at 400 °C for 5 h.

X-ray powder diffraction patterns of the samples were obtained by a model: D8 Diffract meter (Advance, Bruker, Germany), using $\text{Cu K}\alpha$ radiation (1.5406 Å) at 40 kV and 30 mA. The measurements were recorded in steps of 0.045° with a count time of 0.5 s in the range of 2–40°.

Pore size distribution measurements were performed on Autosorb-1 instrument (Quanta chrome, USA) using by nitrogen physisorption.

The UV-vis diffused reflectance spectra were recorded on a GBC UV-visible Cintra 10e spectrometer with an integrating sphere reflectance accessory. The spectra were recorded in air at room temperature and the data was transformed according the Kubelka–Munk equation $f(R) = (1 - R\alpha)/2R\alpha$.

NH_3 -TPD experiments were conducted on the AutoChem 2910 (Micromeritics) instrument. Prior to TPD analysis the sample was pretreated by passing high purity (99.999%) helium (50 ml/min) at 300 °C for 1 h. After pretreatment, the sample was saturated with 10% NH_3 balance He mixture (75 ml/min) at 80 °C for 1 h and subsequently flushed at 150 °C for 1 h to remove the physisorbed ammonia. TPD analysis was carried out from ambient temperature to 700 °C at a heating rate 10 °C/min. The amount of NH_3 desorbed is calculated using GRAMS/32 software.

The ex situ experiments of FT-IR spectra of pyridine adsorbed samples were carried out to find the Brønsted and Lewis acid sites. Pyridine was adsorbed on the activated catalysts at 200 °C until saturation. Prior to adsorption experiments the catalysts were activated in N_2 flow at 300 °C for 1 h to remove adsorbed water in the samples. After such activation, the samples were cooled to room temperature. The IR spectra were recorded using IR (Model: GC-FT-IR Nicolet 670) spectrometer by KBr disk method at room temperature. FT-IR spectra of the catalysts were recorded on IR (Model: GC-FT-IR Nicolet 670) spectrometer by KBr disk method at room temperature.

Thermogravimetry analysis (Shimadzu TGA-51) was measured at a heating rate of 10 °C/min from 25 °C up to 800 °C under the flow of air.

The gas-phase dehydration of glycerol was conducted in the reaction temperature ranging from 280 to 340 °C under atmospheric pressure in a vertical fixed-bed quartz reactor (400 mm length, 9 mm i.d.) using 0.2 g of catalyst. Before the reaction, the catalyst was pretreated at 320 °C for 1 h in flow of dry N_2 (30 mL min⁻¹). An aqueous solution containing 20 wt% glycerol was fed into the reactor by a micro-syringe pump at a flow rate of 0.5 mL/h (WHSV-2.6 h⁻¹). The reaction products were condensed in an ice–water trap and collected hourly for the analysis using a gas chromatograph GC-2014 (Shimadzu) equipped with a DB-wax 123-7033 (Agilent) capillary column (0.32 mm i.d., 30 m long) and a flame ionization detector (FID). The oven temperature was set from 56 °C to 119 °C (heating rate 5 °C/min, isothermal step at 119 °C, 3 min), then from 119 °C to 240 °C (heating rate 15 °C/min, final isothermal step at 240 °C, 6 min).

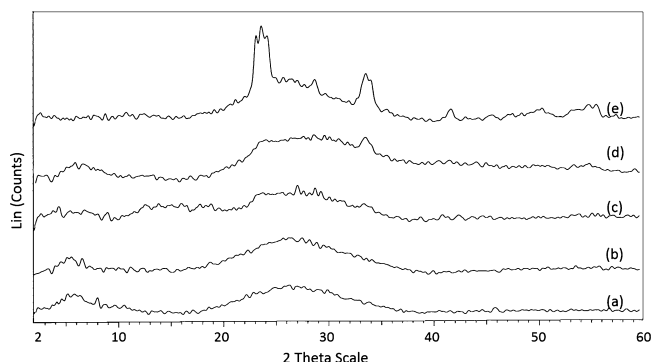


Fig. 1. Powder XRD patterns of pure and tungstated ZrP catalysts. (a) P-ZrP, (b) 10 wt% WO_x/ZrP , (c) 20 wt% WO_x/ZrP , (d) 30 wt% WO_x/ZrP and (e) 40 wt% WO_x/ZrP .

3. Results and discussion

3.1. Catalyst characterization results

X-ray diffraction patterns of various WO_x/ZrP catalysts with tungsten oxide loadings ranging from 10 to 40 wt% are shown in Fig. 1. XRD results suggest that the synthesized ZrP is found to be X-ray amorphous. However, the samples with tungsten oxide loading less than 30 wt% WO_3 , did not show any XRD peaks suggesting that the tungsten oxide is present in a well dispersed amorphous state. However, the samples above 30 wt% WO_3 loadings have shown XRD reflections with poor crystallinity. Additional peaks are observed for the samples with tungsten oxide loading of 40 wt% in the 2θ range of 23–25° [JCPDS-43-1035]. According to the previous studies [22–24], these XRD reflections can be assigned to micro crystallites of monoclinic WO_3 . It has been suggested previously that the agglomeration of WO_x species, leads to WO_3 micro crystallites on the support surface when the tungsten coverage exceeds that of a monolayer [25].

Brunauer–Emmett–Teller (BET) surface area, average pore diameter, and pore volume for pure zirconium phosphate support (ZrP) and tungstated zirconium phosphate (WO_x/ZrP) materials are determined from their respective adsorption isotherms and the results are given in Table 1. The BET surface area of ZrP is found to be $400 \text{ m}^2 \text{ g}^{-1}$ with pore volume of 0.36 cc g^{-1} is comparable to that of previously reported surfactant-templated mesoporous zirconium dioxide [26]. Fig. 2 shows the N_2 adsorption–desorption isotherm of pure ZrP support calcined at 400°C . The isotherm exhibits a high uptake of N_2 at low relative pressures (P/P_0) of 0.1–0.4, suggesting the presence of pore sizes ranging between micropore and mesopore region.

Following impregnation with WO_x , a progressive decrease of surface area and pore volume is observed with increasing WO_x loading (10–40 wt%). Although the surface area and pore volume decreases with WO_x loadings, a high surface area $117 \text{ m}^2 \text{ g}^{-1}$ can be still obtained even after a 30 wt% WO_x loading. This decrease of surface area with increasing WO_x loading probably due to the added WO_x components are occupied in the pores of the ZrP support. As

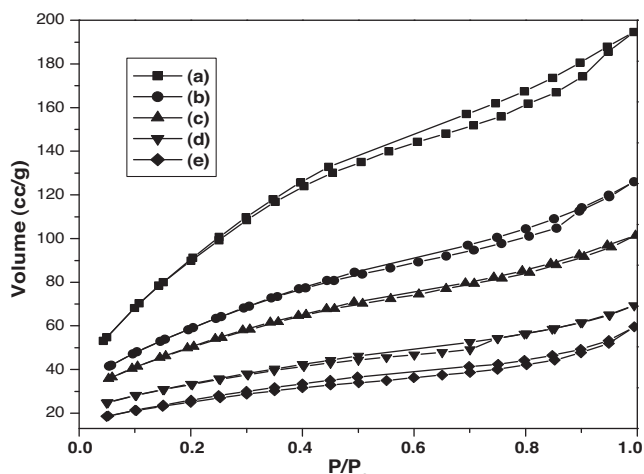


Fig. 2. N_2 adsorption–desorption isotherms of pure and tungstated ZrP catalysts. (a) P-ZrP, (b) 10 wt% WO_x/ZrP , (c) 20 wt% WO_x/ZrP , (d) 30 wt% WO_x/ZrP and (e) 40 wt% WO_x/ZrP .

WO_x loading increases on the ZrP support, the mean pore diameter of the sample is also increasing. However, the isotherms of WO_x/ZrP materials can be classified as type IV, which is a characteristic feature of the mesoporous materials [27]. The isotherm exhibits low uptake of N_2 at low relative pressures (P/P_0) of 0.1–0.4, indicating the decrease of the number of micropore and mesopores compare to pure ZrP. This might be due to filling of the micro pores of ZrP support and these are not included in the measurement. These findings are further confirmed by the pore size distribution profiles shown in the Fig. 3, which reveals a narrow pore size distribution (Fig. 3) centered around 2.2 nm.

UV-vis spectra of all the supported WO_x samples are presented in Fig. 4, along with the spectrum of pure ZrP support. The parent ZrP showed a band at 300 nm due to Zr (IV) cations interacting with the phosphate counter anions in the framework [28]. The UV spectrum of ZrP support is strongly modified by the WO_x species. UV-visible diffuse reflectance spectroscopy was used to probe tungsten oxide species dispersed on zirconia surface. The size effect can be reflected from the shift of the absorption edge [29]. As the WO_x loadings increases on ZrP, the intensity of the charge transfer transition band at 450 nm is also increased, due to characteristic nature of crystalline WO_3 . As described earlier these

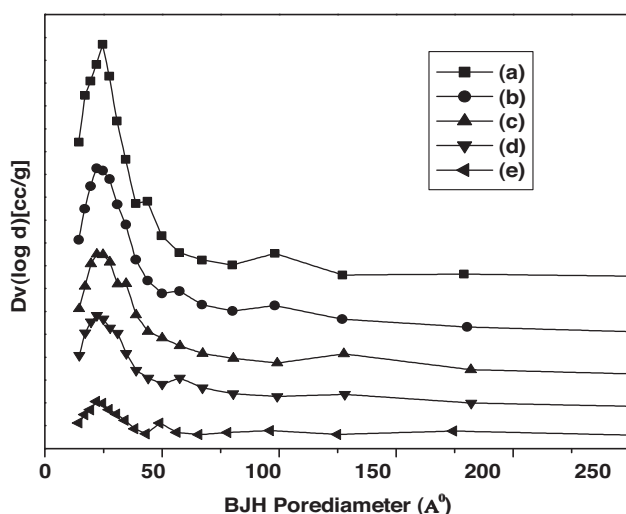


Fig. 3. BJH pore diameter profile of pure and tungstated ZrP catalysts. (a) P-ZrP, (b) 10 wt% WO_x/ZrP , (c) 20 wt% WO_x/ZrP , (d) 30 wt% WO_x/ZrP and (e) 40 wt% WO_x/ZrP .

Table 1

BET surface area and pore size distribution data of pure and tungstated ZrP catalysts.

S. no.	WO_x loadings (wt%)	BET SA ($\text{m}^2 \text{ g}^{-1}$)	Total pore volume (cc/g)	Mean pore diameter (Å)
01	P-ZrP	400	0.36	31.54
02	5W-ZrP	317	0.26	32.53
03	10W-ZrP	236	0.20	33.40
04	20W-ZrP	183	0.16	34.35
05	30W-ZrP	117	0.11	36.70
06	40W-ZrP	99	0.09	41.20

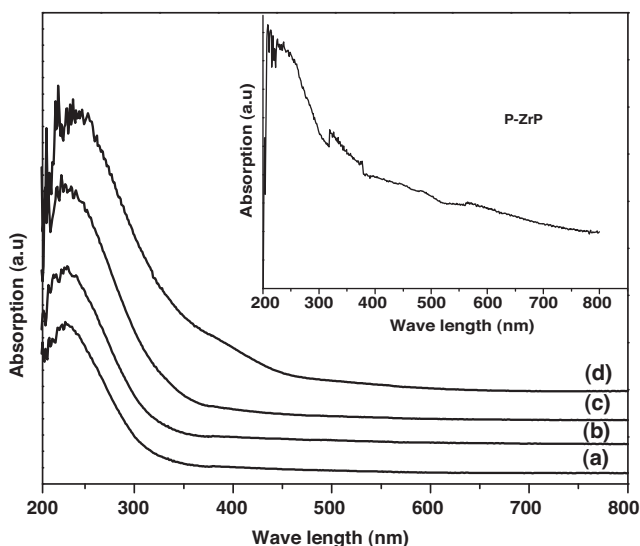


Fig. 4. UV DRS profiles of pure and tungstated ZrP catalysts. (a) 10 wt% WO_x/ZrP , (b) 20 wt% WO_x/ZrP , (c) 30 wt% WO_x/ZrP and (d) 40 wt% WO_x/ZrP .

results are qualitatively in accord with the results obtained from X-ray diffraction.

FT-IR spectra of pure ZrP support and various WO_3/ZrP catalysts are shown in Fig. 5. The spectra of all the samples have shown an absorption band at $1000\text{--}1100\text{ cm}^{-1}$ corresponding to strong Zr–O–P vibration [30]. The IR spectra also show the bands in the region $3400\text{--}2400\text{ cm}^{-1}$ ascribed due to surface OH groups and the IR band at 1630 cm^{-1} is assigned to bending adsorbed mode of water molecule by the catalyst [31]. The absence of band at 750 cm^{-1} suggests the nonexistence of P–O–P (poly phosphate) like groups in pure ZrP [32]. An additional IR band was observed at 820 cm^{-1} in all the impregnated samples, attributable to the W–O_c–W vibration of two connecting WO_6 octahedra. It is also noteworthy that an IR band was observed at 640 cm^{-1} in all the impregnated samples which can be assigned due to a Zr–O vibration. Since this IR band was absent in ZrP support, as it might arise

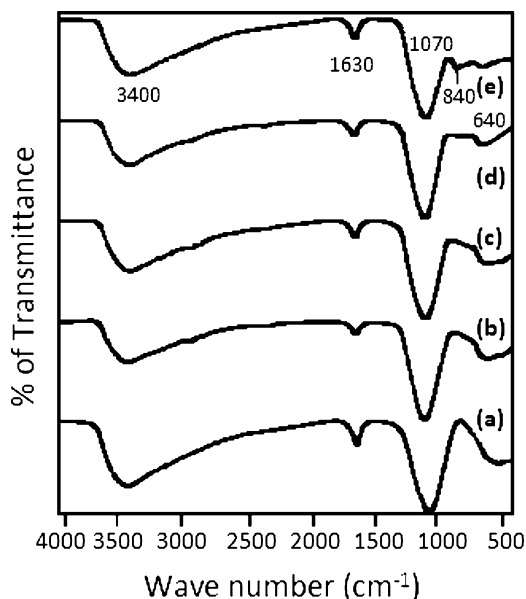


Fig. 5. FT-IR profiles of pure and tungstated ZrP catalysts. (a) P-ZrP, (b) 10 wt% WO_x/ZrP , (c) 20 wt% WO_x/ZrP , (d) 30 wt% WO_x/ZrP and (e) 40 wt% WO_x/ZrP .

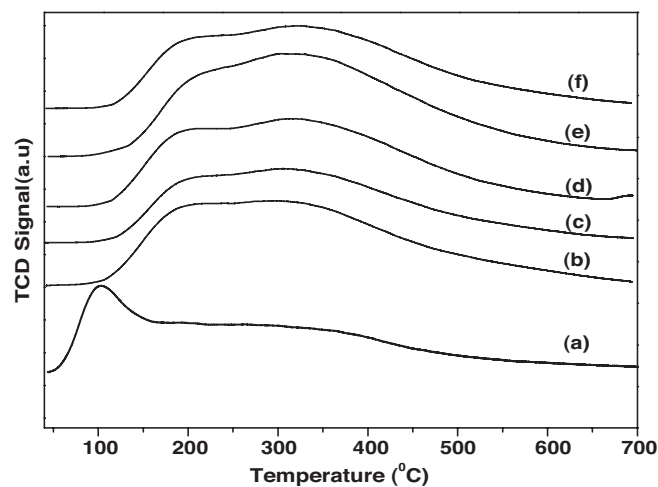


Fig. 6. NH_3 -TPD profiles of pure and tungstated ZrP catalysts. (a) P-ZrP, (b) 5 wt% WO_x/ZrP , (c) 10 wt% WO_x/ZrP , (d) 20 wt% WO_x/ZrP , (e) 30 wt% WO_x/ZrP and (f) 40 wt% WO_x/ZrP .

from a Zr–O–W stretching vibration as postulated by Chauveau et al. [33].

The surface acidity is an important characteristic property of a solid acid catalyst to assess the dehydration functionality of glycerol to acrolein [13]. The ammonia TPD profiles of various loadings of WO_x catalysts supported on ZrP are presented in Fig. 6. The amounts of ammonia desorbed during TPD analysis by various catalysts are shown in Table 2. The pure ZrP support exhibited one sharp peak in the weak acidic region and one broad peak in the moderate acidic region. It can be seen from the Fig. 6 that TPD profiles showed only one broad peak in WO_x/ZrP catalysts. It was difficult for the deconvolution of TPD profiles into weak, moderate and strong acidic sites as the TPD profiles are strongly overlapped. Therefore, the surface acidity was calculated as total acidity and expressed per mol of NH_3 desorbed per gram of catalyst. Additionally, the acidity is given as mol of NH_3 desorbed per m^2 of surface area (Table 2).

The TPD profile shown in Fig. 6 reveals that the desorption peaks are due to weak acidic sites which are present only in ZrP support and no peaks were noticed in WO_x/ZrP catalysts. The total acidity values of supported WO_x on ZrP support are increasing from 5 wt% to 30 wt% WO_x/ZrP and decreases at higher loadings (40 wt% WO_x/ZrP). This could be possibly due to condensation of the W–OH groups and formation of 3-D WO_x clusters at higher WO_x loadings reduces the acidity [34]. However, ammonia is mainly desorbed between 200 and 550°C , in all the WO_x/ZrP catalysts, suggesting the presence of medium and strong acidic sites. The acidity of the WO_x/ZrP catalysts can be attributed to the P–OH and well dispersed WO_x groups present on the surface [35]. TPD analysis suggests that the amount of acidity and strength of acidic sites are increasing upon addition of WO_x ions to the ZrP support.

The previous discussion does not contain any information on the nature of acidic sites, because the ammonia-TPD cannot discriminate Brønsted and Lewis acid sites. For characterizing the nature of

Table 2
Temperature programmed desorption of NH_3 of pure and tungstated ZrP catalysts.

S. no.	WO_x loadings (wt%)	T_{\max} ($^\circ\text{C}$)	NH_3 desorbed (mmol/g)	NH_3 desorbed ($\mu\text{mol}/\text{m}^2$)
01	P-ZrP	120	3.30	8.25
02	5W-ZrP	320	3.72	11.73
03	10W-ZrP	350	3.84	16.25
04	20W-ZrP	350	4.02	21.95
05	30W-ZrP	345	4.91	41.90
06	40W-ZrP	345	4.10	41.00

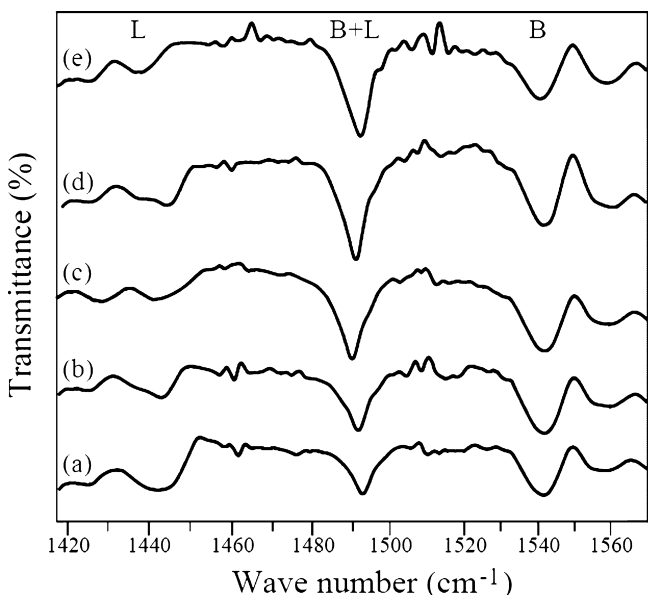


Fig. 7. FT-IR Pyridine adsorption profiles of pure and tungstated ZrP catalysts. (a) P-ZrP, (b) 10 wt% WO_x/ZrP , (c) 20 wt% WO_x/ZrP , (d) 30 wt% WO_x/ZrP and (e) 40 wt% WO_x/ZrP .

surface acidic sites, we have employed ex situ the pyridine adsorbed FT-IR analysis. Prior to ex situ FT-IR analysis the catalyst samples were saturated with pyridine vapour at 200°C for 2 h. The FT-IR analysis reveals that the IR bands appeared at $1540\text{--}1548\text{ cm}^{-1}$ and $1445\text{--}1460\text{ cm}^{-1}$ are characteristic of Brønsted (B) and Lewis (L) acid sites. Furthermore, the IR bands correspond to the combination of both Brønsted and Lewis (B+L) acid sites are appeared at $1490\text{--}1500\text{ cm}^{-1}$. It should be noted that the intensity of the IR bands is proportional to the concentration of acidic sites.

The FTIR spectra of pure ZrP support and various WO_3/ZrP catalysts are illustrated in Fig. 7. All the catalysts have shown IR bands at 1444 cm^{-1} corresponding to Lewis sites and another IR band appeared at 1550 cm^{-1} is attributed to Brønsted sites. It can also be seen from Fig. 7, that all the catalysts contain both Lewis and Brønsted acidic sites in different proportions depending upon the WO_x loadings on the support.

It is interesting to note that with increasing WO_x loadings on the support, the intensity of IR band at 1450 cm^{-1} corresponding to the Lewis acidity decreases marginally. The IR absorption peak at 1498 cm^{-1} is attributed to combination of both Brønsted (B) and Lewis (L) acid sites. This IR peak intensity is increased with increasing WO_x loadings on the support up to 30 wt% WO_x/ZrP . The pure ZrP shows the band at 1550 cm^{-1} due to Brønsted acidic sites. The Brønsted acidity of WO_x/ZrP catalysts increases initially and did not change appreciably until 30 wt% WO_x/ZrP . Furthermore, in 40 wt% WO_x/ZrP a slight decrease of intensity of IR bands is noticed in both the types of acidic sites.

3.2. Catalytic results

The dehydration of glycerol exhibited by various WO_x/ZrP catalysts are illustrated in Figs. 8 and 9 and the product distribution results are reported in Table 3. The influence of the reaction temperature ($280\text{--}340^\circ\text{C}$) on the dehydration of glycerol was examined over 30 wt% WO_x/ZrP by passing air along with N_2 , and the results are shown in Fig. 8. At 280°C the conversion of glycerol is found to be 89% and reaches a maximum at higher temperature. A high selectivity to acrolein formed at moderate temperature can be explained due to the selective activation of the stronger adsorption mode of glycerol through the secondary OH group and the

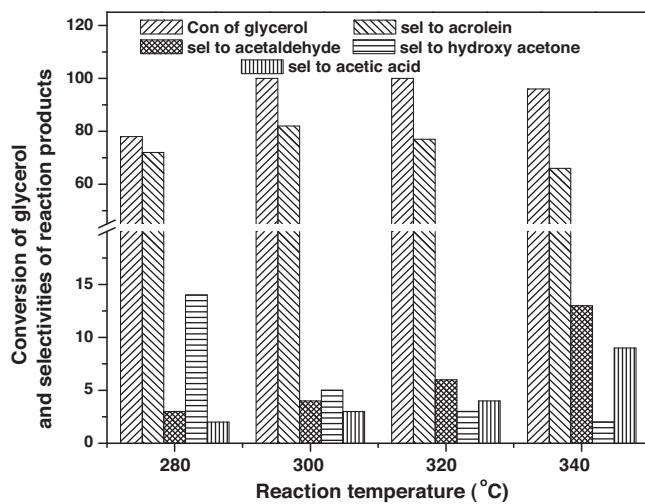


Fig. 8. Effect of reaction temperature on glycerol conversion and selectivity to reaction products on 30 wt% WO_x/ZrP catalyst (reaction conditions: 0.2 g of catalyst was used and diluted with 3.0 g of quartz. The aqueous glycerol (20% wt/wt) was fed at the speed of 0.5 g h^{-1} by B. Braun syringe pump under $7\text{ mL min}^{-1}\text{ N}_2 + 3\text{ mL min}^{-1}$ air atmosphere).

kinetically favored subsequent consecutive steps. Higher amount of hydroxyacetone observed at lower reaction temperature is possibly due to the difference in the activation energies of reaction pathways as depicted in Scheme 1. While the high temperature favors the decomposition of hydroxyacetone, as a result the selectivity of acetaldehyde and acetic acid also increases with reaction temperature.

At 300°C 30 wt% WO_x/ZrP catalyst has shown maximum conversion and selectivity. There is no significant effect on the glycerol conversion is noticed with the increase of temperature (Fig. 8). However, at higher temperature (340°C) the acrolein selectivity decreased due to increase in the formation of acetaldehyde, acetic acid and also a few unidentified products. These results clearly demonstrate that at higher temperature (340°C) the catalyst favors the C–C bond cleavage and also oxidation reaction instead of dehydration of glycerol. The major side product obtained is the acetaldehyde, which is formed due to C–C bond cleavage and oxidation of acetaldehyde leads to the formation of acetic acid. In the view of these findings, 300°C was selected as optimum reaction temperature for screening of the catalysts for further investigation.

The results of the effect of WO_x loading on ZrP support, as well as nature of feed flow (only N_2 and N_2 along with air) during the vapour phase dehydration of glycerol are shown in Table 3. The results clearly suggest that the tungstated zirconium phosphate (WO_x/ZrP) catalysts are found to be more active than pure ZrP support under both the gas flow conditions (only N_2 and N_2 along with air). Glycerol conversion and acrolein selectivity are found to increase with addition of WO_x up to 30 wt% WO_x/ZrP and decreases at higher loadings (40 wt% WO_x/ZrP). The catalysts with 20 wt%, 30 wt% WO_x/ZrP have shown higher glycerol conversion than the other catalysts. However, the sample with 30 wt% WO_x/ZrP exhibited highest selectivity to acrolein (82% using Air + N_2 and 70% using N_2).

Pure ZrP support exhibited 90% glycerol conversion with 52% selectivity toward acrolein under N_2 along with air feed flow. The other products obtained by using pure ZrP support are hydroxyacetone, acetic acid and acetaldehyde as the major by-products along with 32% containing allylic alcohol, acetone, methanol, hydrogenolysis products and also trace amount of unidentified products. The decrease of dehydration activity can be explained by the acidity of P-ZrP support determined with NH_3 -TPD method. The TPD profile

Table 3

Product distribution results of glycerol dehydration over pure and tungstated ZrP catalysts.

S. no.	WO _x loadings (wt%)	Conversion (%)	Selectivity (%)				
			Acrolein	Hydroxy-acetone	Aceticacid	Acetaldehyde	Others
01	P-ZrP	90 [80]	52 [40]	12 [16]	2 [1]	2 [6]	32 [37]
02	5W-ZrP	97 [92]	57 [49]	10 [19]	7 [3]	10 [8]	16 [21]
03	10W-ZrP	100 [95]	62 [55]	7 [17]	12 [3]	10 [10]	9 [15]
04	20W-ZrP	100 [96]	69 [61]	4 [15]	10 [3]	7 [8]	10 [13]
05	30W-ZrP	100 [96]	82 [70]	4 [10]	5 [2]	4 [9]	5 [9]
06	40W-ZrP	95 [90]	74 [68]	6 [12]	7 [2]	5 [7]	8 [11]

Reaction conditions: 0.2 g catalyst was used and diluted with 3.0 g of quartz. The aqueous glycerol (20% wt/wt) was fed at the speed of 0.5 g h⁻¹ by syringe pump under 7 mL min⁻¹ N₂ + 3 mL min⁻¹ Air atmosphere and reaction temperature was 300 °C. The values reported in parenthesis are under similar reaction condition except gas flow of 10 mL min⁻¹ N₂.

of P-ZrP exhibits lower amount of acidity and also the desorption peak appeared at lower temperature region compared to other samples. While zirconia based supports were reported as a neutral materials [36]. It was found that basic sites can exist on its surface along with acidic sites [37]. However, ZrP catalysts have shown excellent acidic properties in many acid catalyzed reactions [32] and it might also contain some basic sites on its surface [38]. The presence of these weak basic sites enables higher selectivity of undesirable products and hydroxyacetone [20,39]. At lower loadings (5 wt% WO_x) these by-products and other products are formed in higher amount because the ZrP support is not fully covered by the WO_x.

The selectivity to hydroxyacetone is found to be very low in WO_x/ZrP catalysts compared to the pure ZrP support suggesting that the addition of WO_x enhances acidity of the catalysts resulting an increase of selectivity of acrolein. The better catalytic performance of these catalysts could imply that the Brønsted acid sites and also catalysts containing both Lewis and the Brønsted acid sites are advantageous for stable acrolein production during glycerol dehydration. Characterization of the WO_x/ZrP catalysts has suggested that the active species correspond to P-OH and W-OH species, which generates Brønsted acid sites active and selective for the dehydration reaction [15,40]. Whereas decrease of catalyst activity at high WO₃ (40 wt %) loading has been attributed to condensation of W-OH groups and formation of 3-D WO_x clusters which lowers the acidity [41]. The XRD results also further support these findings as crystalline WO_x appeared for 40 wt% WO_x/ZrP.

WO_x/ZrO₂ [34,41] and WO_x/ZrP [42] have been used as solid acid catalysts for various reactions, such as esterification, hydrolysis, dehydration, and hydration. The WO_x impregnated catalysts contain stronger acidity and also large number of acidic sites [15,40]. However, such strong acidic catalysts tend to deactivate rapidly as carbonaceous deposits will be formed which blocks the catalyst surface [8,14–16]. Therefore, several attempts were made to control the coke deposition by the co-feeding of molecular oxygen with the feed [43,44]. The positive effect of oxygen gas has been reported previously [45] with the addition of oxygen to the reactant flow. Ulgen and Hoelderich [18] studied the glycerol dehydration reaction over WO_x/ZrO₂ catalyst by passing molecular oxygen with nitrogen gas, and reported that there is an increase in acrolein selectivity and decrease in the main side product selectivity. Wang et al. [43] studied the glycerol dehydration reaction over pure VPO catalyst by passing molecular oxygen with nitrogen gas to maintain the glycerol conversion, acrolein yield and greatly reduces the side product formation. In the present investigation the dehydration of glycerol was carried out over different loadings of WO_x on ZrP support by passing air along with N₂ flow and also only with N₂ feed flow. The effective addition of air in the N₂ flow had a remarkable effect on the catalytic results of glycerol dehydration (Table 3). The results clearly suggest that conversion of glycerol and selectivity to acrolein improved significantly irrespective of active component loading on the support. The presence of air can greatly decreases the selectivity of main side product i.e., hydroxyacetone and other products (mainly allyl alcohol). The selectivity of acetic acid is increasing as it is the oxidation product obtained from secondary reactions. However, there is no significant decrease in the acrolein selectivity. The allyl alcohol is formed by the hydrogenation of acrolein in the reaction medium. The hydrogen is mainly produced from the degradation of glycerol into the coke and addition of air prevents the degradation of glycerol. The hydroxyacetone is produced through the dehydration at the terminal hydroxyl group of glycerol. The oxygen presents in the air restricts the hydrogenation of acrolein and favors the dehydration at the central hydroxyl group of the glycerol.

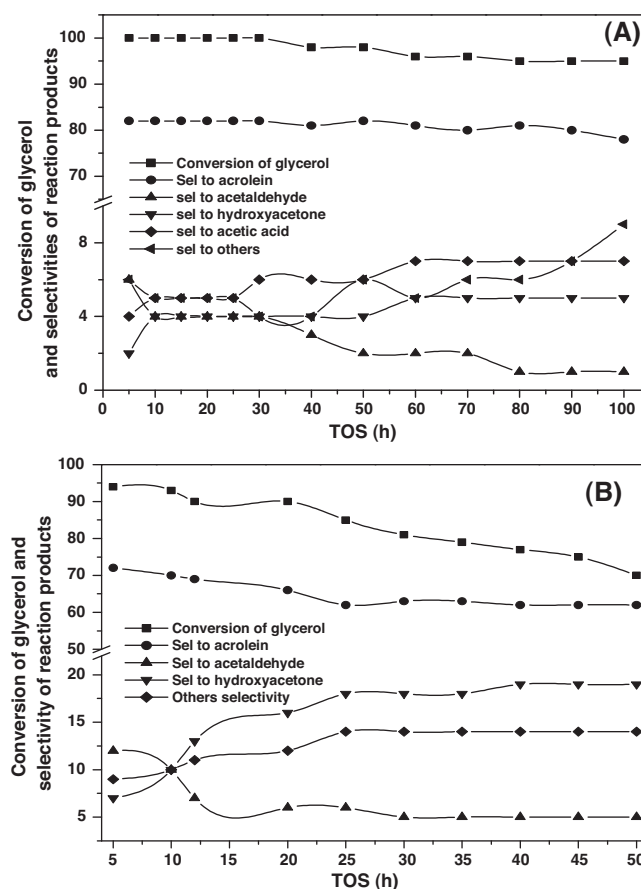


Fig. 9. Evolution of the glycerol conversion and selectivity of reaction products as a function of time over 30 wt% WO_x/ZrP catalyst. (A) By passing 7 mL min⁻¹ N₂ + 3 mL min⁻¹ air flow. (B) By passing 10 mL min⁻¹ N₂. (Reaction conditions: 0.2 g of catalyst was used and diluted with 3.0 g of quartz. The aqueous glycerol (20% wt/wt) was fed at the speed of 0.5 g h⁻¹ by B. Braun syringe pump at 300 °C temperature.).

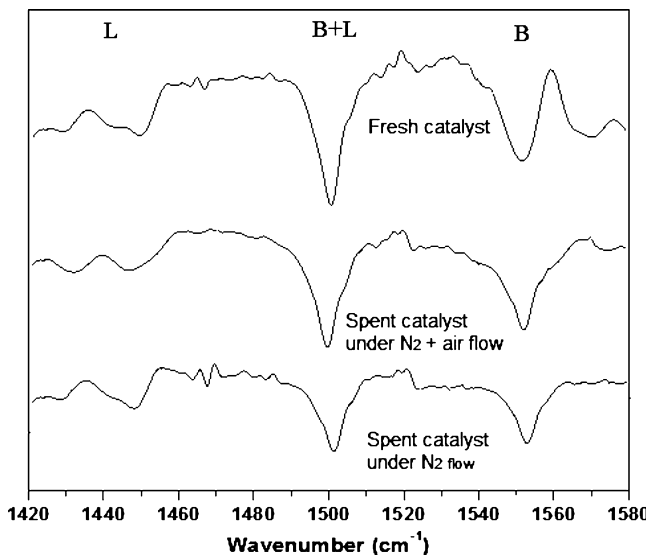


Fig. 10. FT-IR pyridine adsorption profiles of fresh and spent 30 wt% WO_x/ZrP catalysts after 50 h TOS.

The advantage of adding air in the dehydration reaction is not only enriches the selectivity of desired product but also increase life of the catalyst by reducing carbon deposition on the surface of catalyst. Strongly adsorbed hydrocarbon species on the catalyst surface can be quickly removed by oxidation before the formation of intensive carbon coke, and catalytic active sites are recovered.

The effect of feed flow (only N_2 and air along with N_2) over 30 wt% WO_x/ZrP catalyst at 300 °C as a function of reaction time is shown in the Fig. 9 A and B. The results indicate that the conversion of glycerol is found to be greater than 90% even after 100 h of reaction time. Thus by passing N_2 along with air flow enhances the stability of the catalysts during the vapour phase dehydration reaction. However, under only N_2 gas flow (Fig. 9B) a rapid deactivation can be noticed with time on stream (TOS: 50 h–70% conversion). The deactivation phenomenon can be explained by the formation of coke.

During the reaction under only N_2 flow the selectivity to hydroxyacetone increases from 7% to 18% with time on stream. While under the reaction conditions using N_2 along with air flow the selectivity of hydroxyacetone is found to be >6% even after 100 h TOS. However, the acetic acid formation is found to increase in the presence of air in the feed. The change in hydroxyacetone selectivity might depend on the nature of the active sites, which can be modified in situ by the presence of oxygen in the air flow [18]. It is also possible that hydroxyacetone can get oxidized to other products. The selectivities to acetaldehyde initially rather high and decreased with time on stream confirming, that acetaldehyde was formed from consecutive reactions of acrolein or hydroxyacetone in both cases.

Further, the characterization of spent catalysts has provided better explanation on the effect of feed flow during the gas phase dehydration of glycerol. Ex situ pyridine adsorbed FT-IR analysis (Fig. 10) was also performed to examine the acidic properties of the spent (30 wt% WO_x/ZrP) catalysts. The peak areas corresponding to Brønsted (B) and B+L acidic sites of spent catalysts were decreased compared with those of fresh 30 wt% WO_x/ZrP catalyst. However, the spent catalyst under air along with N_2 flow has shown more intense peaks than the spent catalyst under only N_2 flow. This indicates that the addition of air to feed flow regenerate the active sites which are involved in the deactivation during reaction.

The TG-DTG curves of the spent 30 wt% WO_x/ZrP catalysts are shown in Fig. 11. The results suggest that about 10% of weight loss

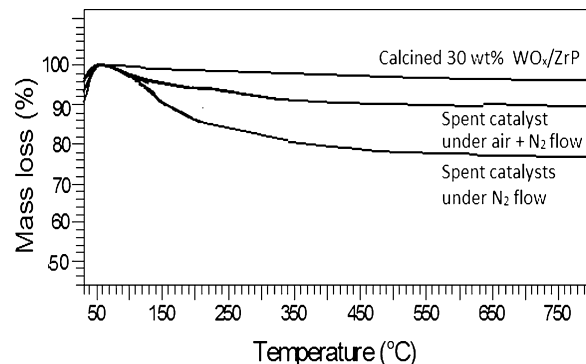


Fig. 11. TG-DTG curve of spent 30 wt% WO_x/ZrP catalysts after 50 h TOS.

Table 4

B.E.T surface area, pore size distribution and CHNS analysis data of NH_3 of fresh and spent 30 wt% WO_x/ZrP catalyst.

	Fresh catalyst	Spent catalyst under Air + N_2	Spent catalyst under N_2 flow
BET surface area ($\text{m}^2 \text{g}^{-1}$)	117.0	55.7	32.4
BJH pore volume (cc/g)	0.11	0.07	0.04
BJH average pore diameter (\AA)	36.7	49.10	61.60
H/C (CHNS analysis)	–	1.48	0.96

occurred at 350 °C after 50 h TOS by passing air along with N_2 . However the spent catalysts under N_2 flow have shown significantly more weight loss (22%) at 450 °C temperature. TGA results further suggest that formation of coke deposited is higher on the surface of 30 wt% WO_x/ZrP catalyst under non aerobic conditions.

Analysis of atomic H/C ratio in the coke over the catalysts reveals that the results are in agreement with findings of the TGA-DTG. The atomic H/C ratio in the coke measured by CHNS elemental analysis (Table 4) was found to be higher for the spent catalyst (30 wt% WO_x/ZrP) under air along with N_2 flow than the spent catalyst under only N_2 flow. The higher H/C ratio of spent catalyst under air along with N_2 flow implies that the carbon deposits have a less condensed and aromatized structure over the active sites.

The results reported in Table 4 suggest that an increase in the average pore diameter is observed in spent 30 wt% WO_x/ZrP catalysts than the fresh catalyst (36.7 Å). This could be possibly due to the pore condensation during the glycerol dehydration reaction leading to deactivation of the catalyst [46]. Interesting observation can be seen from the Table 4 that the average pore diameter significantly increased in the spent catalyst under N_2 (61.6 Å) than the spent catalyst under N_2 along with air flow (49.1). Further, the addition of air to N_2 flow reduces the loss of surface area due to sintering.

4. Conclusions

This study has demonstrated that a series of porous zirconium phosphate supported WO_x catalysts prepared by the wet impregnation method are effective for the gas phase dehydration of glycerol to produce acrolein. The characterization results have confirmed that the WO_x species is well dispersed on ZrP support. The supported WO_x catalyst showed better conversion and selectivity toward acrolein than pure ZrP support. The catalyst performance for the dehydration reaction is significantly affected by the loading of WO_x over the ZrP surface, which induces the changes in the moderate surface acidity and number of Brønsted acidic sites. Improved acidity has been noticed upon addition of WO_3 to ZrP by using NH_3 -TPD and Py-FT-IR techniques. The 30 wt% WO_x/ZrP catalyst has shown the best catalytic performance during glycerol dehydration with 100% conversion and 82% acrolein selectivity compared to

other catalyst. The addition of air during the reaction considerably reduces the formation of by-products and enhances the stability of the catalysts.

Acknowledgment

Author thanks to Council of Scientific and Industrial Research (CSIR-India), New Delhi for the award of Senior Research Fellowship.

References

- [1] S.E. Koonin, *Science* 311 (2006) 435.
- [2] M. Pagliaro, R. Ciriminna, H. Kimura, M. Rossi, C.D. Pina, *Angew. Chem. Int. Ed.* 46 (2007) 4434–4440.
- [3] B. Katryniok, S. Paul, M. Capron, F. Dumeignil, *ChemSusChem* 2 (2009) 719–730.
- [4] D. Arntz, A. Fischer, M. Höpp, S. Jocobi, J. Sauer, T. Ohara, T. Sato, N. Shimizu, H. Schwind, *Ullmann's Encyclopedia of Industrial Chemistry*, 17, 7th ed., Wiley-VCH, Weinheim, 2012, pp. p329.
- [5] C. Zhao, I.E. Wachs, *Catal. Today* 118 (2006) 332–343.
- [6] M.J. Antal, W.S.L. Mok, J.C. Roy, A.T. Raissi, *J. Anal. Appl. Pyrol.* 8 (1985) 291–303.
- [7] S. Chai, H. Wang, Y. Liang, B. Xu, *Green Chem.* 9 (2007) 1130–1140.
- [8] J. Lourenco, M.I. Macedo, A. Fernandes, *Catal. Commun.* 19 (2012) 105–109.
- [9] B. Katryniok, S. Paul, V. Bellière-Baca, P. Rey, F. Dumeignil, *Green Chem.* 12 (2010) 2079–2098.
- [10] C.J. Jia, Y. Liu, W. Schmidt, A.H. Lu, F. Schüth, *J. Catal.* 269 (2010) 71–79.
- [11] Y.T. Kim, K.D. Jung, E.D. Park, *Micropor. Mesopor. Mater.* 131 (2010) 28–36.
- [12] E. Tsukuda, S. Sato, R. Takahashi, T. Sodesawa, *Catal. Commun.* 8 (2007) 1349–1350.
- [13] B. Katryniok, S. Paul, M. Capron, C. Lancelot, V. Bellière-Baca, P. Rey, F. Dumeignil, *Green Chem.* 12 (2010) 1922–1930.
- [14] N.R. Shiju, D.R. Brown, K. Wilson, G. Rothenberg, *Top. Catal.* 53 (2010) 1217–1220.
- [15] A. Alhanash, E.F. Kozhevnikova, I.V. Kozhevnikov, *Appl. Catal. A: Gen.* 378 (2010) 11–18.
- [16] A. Witsuthammakul, T. Sooknoi, *Appl. Catal. A: Gen.* 413–414 (2012) 109–116.
- [17] C.H. Zhou, J.N. Beltramini, Y.X. Fan, C.Q. Lu, *Chem. Soc. Rev.* 37 (2008) 527–549.
- [18] A. Ulgen, W. Hoelderich, *Catal. Lett.* 131 (2009) 122–128.
- [19] J.L. Dubois, C. Duquenne, W. Hoelderich, J. Kervennal, WO2006087084, 2006.
- [20] P.L. Garbey, S. Loridant, V.B. Baca, P. Rey, J.M.M. Millet, *Catal. Commun.* 16 (2011) 170–174.
- [21] T.Z. Ren, Z.Y. Yuan, B.L. Su, *Chem. Commun.* (23) (2004) 2730–2731.
- [22] A. Martinez, G. Prieto, M.A. Arribas, P. Concepcion, *Appl. Catal. A: Gen.* 309 (2006) 224–236.
- [23] A. Martinez, G. Prieto, M.A. Arribas, P. Concepcion, J.F. Sanchez- Royo, *J. Catal.* 248 (2007) 288–302.
- [24] S. Sarish, B.M. Devassy, S.B. Halligudi, *J. Mol. Catal. A: Chem.* 235 (2005) 44–51.
- [25] N. Liu, S. Ding, Y. Cui, N. Xue, L. Peng, X. Guo, W. Ding, *Chem. Eng. Res. Des.* 91 (2013) 573–580.
- [26] Z.Y. Yuan, A. Vantomme, A. Leonard, B.L. Su, *Chem. Commun.* (13) (2003) 1558–1559.
- [27] J. Jiménez-Jiménez, P. Maireles-Torres, P. Olivera-Pastor, E. Rodríguez-Castellón, A. Jiménez-López, D.J. Jones, J. Rozire, *Adv. Mater.* 10 (1998) 812–815.
- [28] M. Ziyad, M. Rouimi, J.L. Portefaix, *Appl. Catal. A: Gen.* 183 (1999) 93–105.
- [29] G.A. Ozin, S. Ozkar, *J. Phys. Chem.* 94 (1990) 7556–7560.
- [30] H.N. Kim, S.W. Keller, T.E. Mallouk, J. Schmitt, G. Decher, *Chem. Mater.* 9 (1997) 1414–1421.
- [31] A. Clearfield, D.S. Thakur, *Appl. Catal.* 26 (1986) 1–26.
- [32] A. Sinhamahapatra, N. Sutradhar, B. Roy, A. Tarafdar, H.C. Bajaj, A. Baran Panda, *Appl. Catal. A: Gen.* 385 (2010) 22–30.
- [33] F. Chauveau, J. Eberle, J. Lefebvre, *Nouv. J. Chim.* 9 (1985) 315–319.
- [34] A. Kumara, A. Alia, K.N. Vinoda, A. Kumar Mondal, H. Hegde, A. Menon, B.H.S. Thimmappa, *J. Mol. Catal. A: Chem.* 378 (2013) 22–29.
- [35] T.Y. Kim, D.S. Park, Y. Choi, J. Baek, J.R. Park, J. Yi, *J. Mater. Chem.* 22 (2012) 10021–10028.
- [36] J. Goscianska, M. Ziolek, E. Gibson, M. Daturi, *Catal. Today* 152 (2010) 33–41.
- [37] K. Pokrovski, K.T. Jung, A.T. Bell, *Langmuir* 17 (2001) 4297–4300.
- [38] D. Spielbauer, G.A.H. Mekheimer, T. Riemer, M.I. Zaki, H. Knozinger, *J. Phys. Chem. B* 101 (1997) 4681–4690.
- [39] A.K. Kinage, P.P. Upare, P. Kasinathan, Y.K. Hwang, J.S. Chang, *Catal. Commun.* 11 (2010) 620–623.
- [40] Y.T. Kim, K.D. Jung, E.D. Park, *Appl. Catal. B: Environ.* 107 (2011) 177–187.
- [41] S.T. Wong, T. Li, S. Cheng, J.F. Lee, C.Y. Mou, *J. Catal.* 215 (2003) 45–56.
- [42] K. Narasimha Rao, A. Sridhar, A.F. Lee, S.J. Tavener, N.A. Young, K. Wilson, *Green Chem.* 8 (2006) 790–797.
- [43] F. Wang, J.L. Dubois, W. Ueda, *Appl. Catal. A: Gen.* 376 (2010) 25–32.
- [44] A. Corma, G.W. Huber, L. Sauvanaud, P. O'Connor, *J. Catal.* 257 (2008) 163–171.
- [45] J.L. Dubois, C. Duquenne, W.H. Hoelderich, 2005, F Patent 2,882,052 to Arkema, SA.
- [46] C. Hulteberg, A. Leveau, J.G. Meo Brandin, *Top. Catal.* 56 (2013) 813–821.